


RESEARCH

Open Access



# Metabolic synthetic lethality by targeting NOP56 and mTOR in *KRAS*-mutant lung cancer

Zhang Yang<sup>1†</sup>, Shun-Qing Liang<sup>1,2†</sup>, Liang Zhao<sup>1</sup>, Haitang Yang<sup>1,3</sup>, Thomas M. Marti<sup>1</sup>, Balazs Hegedüs<sup>4</sup>, Yanyun Gao<sup>1</sup>, Bin Zheng<sup>5</sup>, Chun Chen<sup>5</sup>, Wenxiang Wang<sup>6</sup>, Patrick Dorn<sup>1</sup>, Gregor J. Kocher<sup>1</sup>, Ralph A. Schmid<sup>1\*</sup> and Ren-Wang Peng<sup>1\*</sup> 

## Abstract

**Background:** Oncogenic *KRAS* mutations are prevalent in human cancers, but effective treatment of *KRAS*-mutant malignancies remains a major challenge in the clinic. Increasing evidence suggests that aberrant metabolism plays a central role in *KRAS*-driven oncogenic transformation. The aim of this study is to identify selective metabolic dependency induced by mutant *KRAS* and to exploit it for the treatment of the disease.

**Method:** We performed an integrated analysis of RNAi- and CRISPR-based functional genomic datasets ( $n = 5$ ) to identify novel genes selectively required for *KRAS*-mutant cancer. We further screened a customized library of chemical inhibitors for candidates that are synthetic lethal with NOP56 depletion. Functional studies were carried out by genetic knockdown using siRNAs and shRNAs, knockout using CRISPR/Cas9, and/or pharmacological inhibition, followed by cell viability and apoptotic assays. Protein expression was determined by Western blot. Metabolic ROS was measured by flow cytometry-based quantification.

**Results:** We demonstrated that nucleolar protein 5A (NOP56), a core component of small nucleolar ribonucleoprotein complexes (snoRNPs) with an essential role in ribosome biogenesis, confers a metabolic dependency by regulating ROS homeostasis in *KRAS*-mutant lung cancer cells and that NOP56 depletion causes synthetic lethal susceptibility to inhibition of mTOR. Mechanistically, cancer cells with reduced NOP56 are subjected to higher levels of ROS and rely on mTOR signaling to balance oxidative stress and survive. We also discovered that IRE1 $\alpha$ -mediated unfolded protein response (UPR) regulates this process by activating mTOR through p38 MAPK. Consequently, co-targeting of NOP56 and mTOR profoundly enhances *KRAS*-mutant tumor cell death in vitro and in vivo.

**Conclusions:** Our findings reveal a previously unrecognized mechanism in which NOP56 and mTOR cooperate to play a homeostatic role in the response to oxidative stress and suggest a new rationale for the treatment of *KRAS*-mutant cancers.

**Keywords:** *KRAS*-mutant cancer, NOP56, mTOR, ROS, Synthetic lethal vulnerability

## Background

Oncogenic mutations in the *RAS* family (*HRAS*, *KRAS*, and *NRAS*) are the most common genetic alterations across human cancers and occur in approximately 25% of all tumors (COSMIC; <http://cancer.sanger.ac.uk/cosmic>). *KRAS* is the predominant isoform of the *RAS* family proteins activated by mutations (most frequently at codon 12, 13, and 61) in cancers and is responsible for 85% of all

\*Correspondence: [Ralph.Schmid@insel.ch](mailto:Ralph.Schmid@insel.ch); [Renwang.Peng@insel.ch](mailto:Renwang.Peng@insel.ch)

<sup>†</sup>Zhang Yang and Shun-Qing Liang contributed equally to this work.

<sup>1</sup> Division of General Thoracic Surgery and Department of BioMedical Research (DBMR), Inselspital, Bern University Hospital, University of Bern, Murtenstrasse 28, 3008 Bern, Switzerland

Full list of author information is available at the end of the article



RAS-driven cancers, particularly pancreatic, colon, and non-small cell lung cancer (NSCLC) [1]. Mutant KRAS is associated with poor prognosis and treatment resistance. However, unlike NSCLC with less frequent oncogenic drivers (e.g., EGFR, ALK, MET1, and ROS1) that respond significantly to selective kinase inhibitors [2], effective therapies specifically targeting *KRAS*-mutant cancers remains a challenge [2, 3]. Despite recent progress of immune checkpoint inhibitors of programmed death 1 (PD1) and the ligand PD-L1 in treating NSCLC, they fail to discriminate *KRAS*-mutant from other NSCLC [4]. Covalent KRAS inhibitors have demonstrated promise in preclinical models, but they are only effective for a specific *KRAS-G12C* mutant allele and additional agents are needed to optimize the anticancer efficacy [5–7]. Targeting KRAS downstream effectors, such as the mitogen-activated protein kinase (MAPK) RAF/MEK/ERK, has been widely pursued, but the pleiotropic nature and complex interplay among individual signaling cascades and toxicity ensuing from sustained inhibition of multiple KRAS effector pathways has hindered the translational potential of the strategy [8, 9]. Consequently, identification of new targets for innovative treatment strategies tailored to *KRAS*-mutant cancers still represents a pressing need [3].

The concept to target KRAS synthetic lethality, premised by the notion that oncogenic KRAS signaling fuels a unique cell state, manifested by adaptation to oncogenic stress and transcriptional, translational and metabolic reprogramming, and that interfering with this *KRAS*-driven cell state may result in selective cytotoxicity for *KRAS*-mutant cancer, provides an alternative strategy for treating *KRAS*-driven cancers [10, 11]. Indeed, exploiting cancer cell vulnerabilities contextually induced by mutant KRAS, in particularly the mechanisms critical for surveillance of oncogene-dependent cellular stresses (genotoxic, proteotoxic, and metabolic) that are permissive for strong oncogenic signaling, has not only provided promising therapeutic avenues but also a wealth of information on the fundamental principles of KRAS-induced tumorigenicity [12–14]. Activating *KRAS* mutations deregulate mitosis, nuclear export, redox, and mitochondrial activity, and *KRAS*-mutant cancer cells have consequently been shown to have a greater dependency on the functions of non-oncogenes [e.g., PLK1, XPO1, and MRPL52 (a component of the mitochondrial large ribosomal subunit)] that play critical roles in their respective processes [12–16], suggesting that targeting non-oncogene addiction is an attractive approach for the treatment of *KRAS*-mutant cancer [17, 18].

NOP56 (nucleolar protein 5A or NOL5A) is a ribonuclear protein, which, together with fibrillarin (FBL), NOP58 (nucleolar protein 58), and nonhistone

chromosome protein 2-like 1 (NHP2L1 or SNU13p, 15.5kDa), forms the core protein set of box C/D small nucleolar ribonucleoprotein complexes (snoRNPs) that play an essential role in ribosome assembly by methylating rRNA at the 2'-O-ribose and modulating ribosomal RNA (rRNA) processing [19, 20]. Recent evidence suggests that NOP56 and the other snoRNPs are the novel group of nucleolar proteins that promote cell transformation and tumorigenesis [21, 22]. Indeed, ribosome biogenesis is the only cellular process in which a large number of genes harbor evolutionarily conserved MYC-binding sites [21]. NOP56 is overexpressed in Burkitt's lymphoma and other cancers and serves as a marker of poor prognosis [23]. In particular, NOP56 is required for MYC-induced cell transformation and tumor growth in Burkitt's lymphoma [21]. NOP56 may also have extraribosomal functions that remain to be discovered. Nevertheless, the activity of snoRNPs in oncogenic transformation suggests that they are promising therapeutic targets for cancer treatment [24, 25].

In this study, we reported an unexpected function of NOP56 in metabolic stress response and a previously unrecognized metabolic synthetic lethality by targeting NOP56 and mTOR in *KRAS*-mutant cancers. Based on integrated analyses of RNAi- and CRISPR-mediated functional genomics [12, 16, 26], we identified NOP56 as a novel metabolic dependency of *KRAS*-mutant cancer by regulating homeostasis of reactive oxygen species (ROS) that plays a well-established role in mutant *KRAS*-induced tumorigenesis [27–30]. Depletion of *NOP56* impairs the response to oxidative stress, which renders *KRAS*-mutant cancer cells highly dependent on mTOR signaling for survival and particularly vulnerable to mTOR inhibition. Consequently, co-targeting NOP56 and mTOR enhances apoptotic death of *KRAS*-mutant lung cancer cells in vitro and in vivo. We further delineated that mTOR activation upon NOP56 depletion is mediated by IRE1 $\alpha$ -mediated unfolded protein response (UPR). These results uncover a previously unknown mechanism by which NOP56 cooperates with UPR and mTOR to regulate metabolic stress and a novel synthetic lethal strategy for the treatment of *KRAS*-mutant cancers.

## Materials and methods

### Cell culture and reagents

Cancer cell lines used in this study (Table S1) were obtained from American Type Culture Collection (ATCC, Manassas, VA, USA). Cells were cultured in RPMI-1640 medium or Medium 199 (Cat. #8758 and #4540; Sigma-Aldrich, St. Louis, MO, USA) supplemented with 10% fetal bovine serum/FBS (Cat. #10270–106; Life Technologies, Grand Island, NY, USA)

and 1% penicillin/streptomycin solution (Cat. #P0781, Sigma-Aldrich). The cells were authenticated by DNA fingerprinting and confirmed free from mycoplasma contamination (Microsynth, Bern, Switzerland). All inhibitors used in this study were listed in Table S2.

PF139 and PF563 lung cancer cells were established from lung adenocarcinoma malignant pleural effusion and pleural carcinosis specimens of a 67-year-old female patient and a 75-year-old male patient, respectively, at the time of diagnosis prior to any treatment [31]. Authentication was performed by SNP based cell identification (Multiplexion, Heidelberg, Germany).

#### Cell viability and clonogenic survival assay

Lung cancer cells seeded in 96-well plates (2500 cells/well) were dosed 24 h later with different inhibitors for 72 h. Cell viability was determined by PrestoBlue (PB) Cell Viability Reagent (ThermoFisher Scientific) by following the manufacturer's instructions [14, 31]. The PB reagent was added into media directly (1:10 dilution) and incubated for 30 min–2 h and then the fluorescence was read (excitation 570 nm; emission 600 nm) at recommended time of incubation. The efficacy of drugs on cell growth was normalized to untreated control. Each data point was generated in triplicate and each experiment was done three times ( $n=3$ ). Best-fit curve was generated in GraphPad Prism [(log (inhibitor) vs response (–variable slope four parameters)]. Error bars are mean  $\pm$  SD. The combination index (CI) was calculated by ComboSyn software (ComboSyn Inc., <http://www.combosyn.com/>).

Clonogenic assay was done as we described previously [14, 31–33]. In brief, cells seeded in 6-well plates (3000 cells/well) were dosed 24 h later and continually treated with rapamycin for 7 days (refresh drugs every 3 days), the resulting colonies were stained with crystal violet (0.5% dissolved in 25% methanol).

#### Apoptosis assays

Lung cancer cells were treated for 72 h with vehicle or rapamycin. After treatment, cells in the supernatant and adherent to plates were collected, washed with PBS and pooled before suspended in binding buffer and stained with the Annexin V Apoptosis Detection Kit -FITC (Cat. #88–8005; Thermo Fisher Scientific, Waltham, MA, USA) according to the manufacturer's instructions. Flow cytometry analysis was performed on a BD Biosciences LSRII flow cytometer.

#### Gene silencing by small interfering (siRNA), short hairpin RNAs (shRNA) and single-guide RNAs (sgRNA)

Transient knockdowns were mediated by siRNAs. Cells cultured in triplicate at 50–70% confluency were transfected using SiTran1.0 (TT300001; Origene

Technologies, Rockville, MD, USA) according to the manufacturer's protocol. *NOP56* (CAT#: SR307156), *EIF4E* (CAT#: SR320018), *RPS6* (CAT#: SR304160), *RAPTOR* (CAT#: SR324724), and *RICTOR* (CAT#: SR326062) were knocked down by specific pooled siRNA duplexes purchased from OriGene Technologies, with control siRNA Duplex as a negative control.

Stable knockdown of *NOP56* was achieved via lentiviral delivery of *NOP56* Human shRNA Plasmid Kit (SHCLND\_006392, MERCK). A scramble shRNA was used as a control. Lentiviral particles were generated and cells infected according to the protocol from Broad Institute. The supernatant containing lentiviruses was collected, filtered through 0.45  $\mu$ M filters, and stored in aliquots at  $-80^{\circ}\text{C}$ , or immediately used to infect recipient cells. After infection, cells were selected in puromycin (1.5  $\mu$ g/ml) and further passaged in culture for functional assays. *NOP56* knockout was performed via a CRISPR/Cas9 and non-homology mediated approach using the NOL5A (*NOP56*) Human Gene Knockout Kit (CAT#: KN411153; OriGene Technologies) according to the manufacturer's protocol.

#### Quantitative real-time PCR (qRT-PCR)

Total RNA was isolated and purified using RNeasy Mini Kit (Qiagen, Hilden, Germany). Complementary DNA was synthesized by the High capacity cDNA reverse transcription kit (Applied Biosystems, Foster City, CA, USA) according to manufacturer's instructions. Real time PCR was performed in triplicate on a 7500 Fast RealTime PCR System (Applied Biosystems) using TaqMan primer/probes (Applied Biosystems): *HSPA5*, Hs00607129\_gH; *ERN1*, Hs00980095\_m1; *EIF2AK3*, Hs00984003\_m1; *ATF4*, Hs00909569\_g1; *DDIT3*, Hs00358796\_g1, with *GAPDH* (Hs02786624\_g1) and *ACTB* (Hs01060665\_g1) used as endogenous normalization controls.

#### Immunoblotting, immunohistochemistry and immunofluorescence

Cell lysates were prepared and western blot analysis was performed as described [14, 31]. In brief, equal amounts of protein lysates resolved by SDS-PAGE (Cat. #4561033; Bio-Rad Laboratories, Hercules, CA, USA) and transferred onto nitrocellulose membranes (Cat. #170–4158; Bio-Rad). Membranes were then blocked with blocking buffer (Cat. #927–4000; Li-COR Biosciences, Bad Homburg, Germany) for 1 h at room temperature (RT) and incubated with appropriate primary antibodies overnight at  $4^{\circ}\text{C}$  (Table S3). IRDye 680LT-conjugated goat anti-mouse IgG (Cat. #926–68,020) and IRDye 800CW-conjugated goat anti-rabbit IgG (Cat. #926–32,211) from Li-COR Biosciences were used at 1:5000 dilutions. Finally, signals of membrane-bound secondary antibodies

were imaged using the Odyssey Infrared Imaging System (Li-COR Biosciences).

For immunofluorescence, tumor cells grown on polylysine-treated coverslides were fixed with 4% paraformaldehyde for 15 min at RT and permeabilized with cold methanol ( $-20^{\circ}\text{C}$ ) for 5 min or with 0.1% Triton X-100/PBS at RT for 15 min before incubated overnight at  $4^{\circ}\text{C}$  with primary antibodies (Table S3). The cells were incubated for 1 h at RT with Alexa Fluor 647 goat anti-mouse IgG (Cat. #A21236) or Alexa Fluor 488 goat anti-Rabbit IgG (Cat. #A11034) from Invitrogen (Eugene, OR, USA). Nuclei were counterstained by 4',6-diamidino-2-phenylindole. Images were acquired on a ZEISS Axioplan 2 imaging microscope (Carl Zeiss MicroImaging, Göttingen, Germany) and processed using Adobe Photoshop CS6 v.13 (Adobe Systems, San Jose, CA, USA).

Immunohistochemical study was performed as we described previously [31, 32]. In brief, surgically removed xenograft tumors were formalin-fixed and paraffin-embedded (FFPE). FFPE tumors were sectioned at  $4\ \mu\text{m}$ , deparaffinized, rehydrated and subsequently stained with hematoxylin and eosin (H&E) and appropriate antibodies (Table S3) using the automated system BOND RX (Leica Biosystems, Newcastle, UK). Visualization was performed using the Bond Polymer Refine Detection kit (Leica Biosystems) as instructed by the manufacturer. Images were acquired using PANNORAMIC® whole slide scanners, processed using Case Viewer (3DHISTECH Ltd.). The staining intensities of the whole slide (two tumors/group) were quantified by QuPath software.

### In vivo mouse study

Mouse studies were conducted in accordance with Institutional Animal Care and Ethical Committee-approved animal guidelines and protocols. All mouse experiments were performed in age- and gender-matched NSG (NOD-*scid* IL2R $\gamma^{null}$ ) as we previously described [31, 32]. Tumor cells in DMEM (H460-shScrambled or H460-shNOP56) 1:1 mixed with BD Matrigel Basement Membrane Matrix (Cat. #356231; Corning, NY, USA)

were subcutaneously inoculated in left and right flanks ( $0.5 \times 10^6$ /injection). When tumors were palpable, mice were randomly assigned to treatment groups: 1) control; 2) rapamycin (0.1 mg/kg, i.p, 5 days/week) for 5 weeks. Tumors were measured every 3 days, with their size calculated as follows:  $(\text{length} \times \text{width}^2)/2$ . For survival analysis, the mice were closely monitored on a daily basis, and the size of tumors was measured with a caliper every 4–5 days. Mice were sacrificed when the tumor volume reached  $1500\ \text{mm}^3$ .

### Public databases

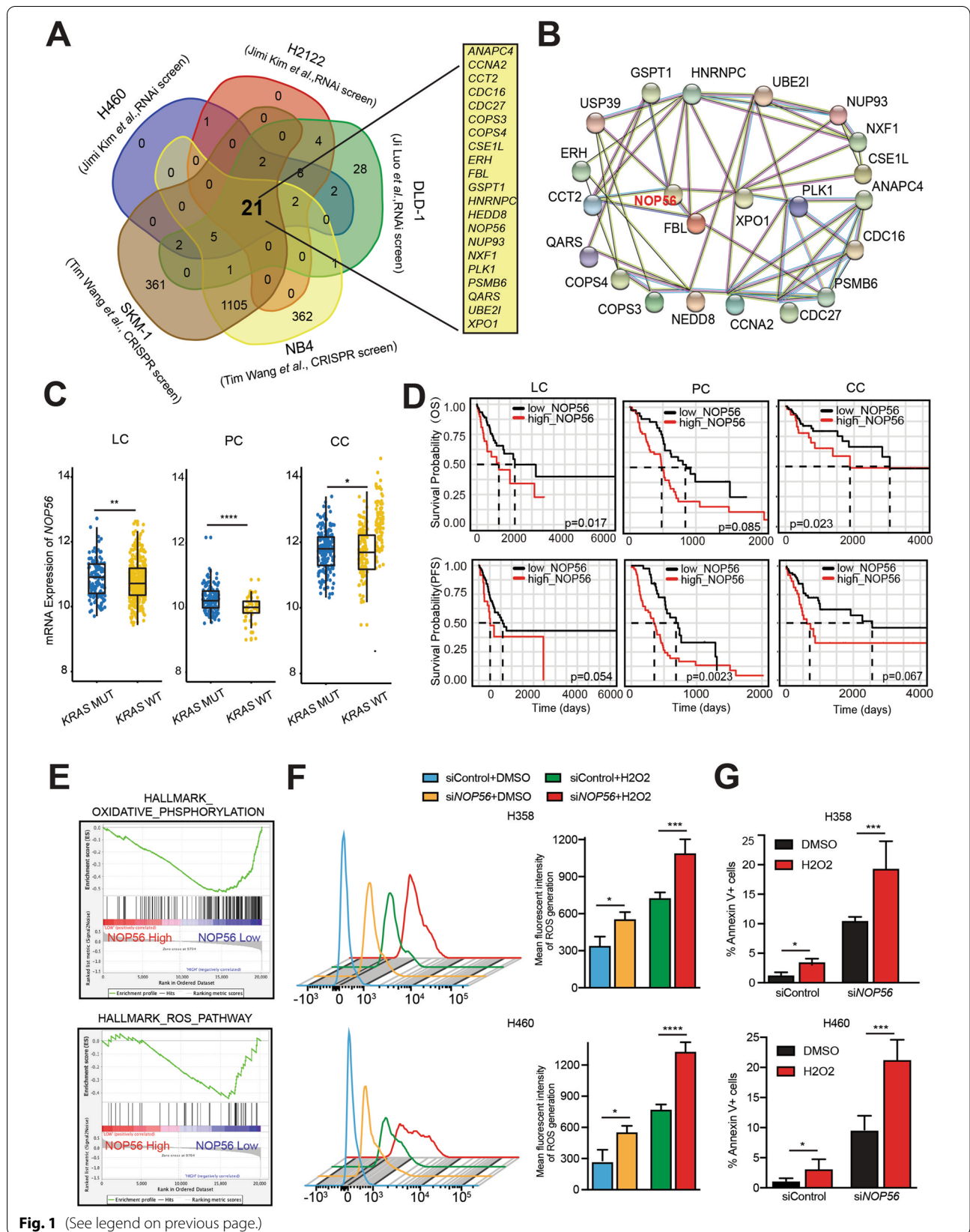
To identify synthetic lethal targets in *KRAS*-mutant cancers, we interrogated functional genomics dataset of CRISPR/Cas9 knockout and RNAi/shRNA knockdown screens from published studies: whole genome RNAi screens in DLD-1 colon cancer cells [12] and in *KRAS*-mutant lung cancer cells (H2122, H2009, HCC44, H460, H1155) [16], genome-wide CRISPR/Cas9 loss of function screens in *KRAS*-mutant leukemia cells (PL-21, SKM-1, NB4) [26]. To minimize the effects of cancer lineage and histological subtype, we selected DLD-1 (colon), H460 (large cell lung carcinoma), H2122 (lung adenocarcinoma), SKM-1 (without *PML-RARA* fusion) and NB4 (*PML-RARA*) for further analysis, which identified a number of common candidates ( $n = 21$ ) as *KRAS* synthetic lethal partners (Fig. 1).

Interrogation of publicly available datasets was performed as we have described [14, 31]. Specifically, transcriptomic data of lung, pancreatic and colon cancer were obtained from the Cancer Genome Atlas (TCGA) (<https://portal.gdc.cancer.gov/projects/TCGA>). Gene set enrichment analysis (GSEA) was performed by using GSEA software. The transcriptomic dataset (GSE15212) used for GSEA was derived from *KRAS*-mutant colon cancer cell line (SW480) treated with *NOP56*-specific siRNAs and downloaded from the Gene Expression Omnibus (GEO) database. For survival analysis, transcriptomic gene expression and corresponding survival data were extracted and analyzed by using the “maxstat”, “survival”, and “survminer” packages in R software

(See figure on next page.)

**Fig. 1** NOP56 confers a metabolic dependency in *KRAS*-mutant cancers. **A**, Venn diagram showing common essential genes in *KRAS*-mutant cancer cells. Data are based on the published studies, with the 21 common genes listed on the right. **B**, Network analysis of the 21 common genes by STRING. **C**, *NOP56* mRNA expression in *KRAS*-mutant lung cancer (LC), pancreatic cancer (PC) and colon cancer (CC) versus *KRAS*-wild-type (WT) cancers in patient samples from TCGA. **D**, Prognostic values of *NOP56* expression across TCGA lung adenocarcinoma (left), pancreatic cancer (middle) and colon cancer (right) cohorts harboring *KRAS* mutations. Kaplan–Meier survival analyses were stratified by the optimal cut-off value of *NOP56* mRNA levels. **E**, Gene set enrichment analysis (GSEA) revealed significant enrichment of oxidative phosphorylation and ROS pathway gene signatures in *NOP56*-depleted *KRAS*-mutant cancer cells (SW480). The GEO dataset GSE15212 was used for GSEA. **F**, H358 and H460 cells transfected with *NOP56*-specific or control siRNAs were treated (72 h post-transfection) with  $300\ \mu\text{M}$   $\text{H}_2\text{O}_2$  for 6 h, followed by incubation with H2DCFDA for 30 min, and analyzed by flow cytometry. Quantification of relative ROS levels was shown in the right. Data are shown as the mean  $\pm$  SD ( $n = 3$ ). \* $P < 0.05$ , \*\*\* $P < 0.001$ , \*\*\*\* $P < 0.0001$  by two-way ANOVA with Tukey's multiple comparisons test. **G**, H358 and H460 cells transfected with *NOP56*-specific or control siRNAs were subsequently (72 h post transfection) treated with vehicle (DMSO) or  $300\ \mu\text{M}$   $\text{H}_2\text{O}_2$  for 6 h before apoptotic assay. Data were shown as mean  $\pm$  SD ( $n = 3$ ). \* $P < 0.05$  and \*\*\*\* $P < 0.001$  by two-way ANOVA with Tukey's multiple comparisons test





(version 3.6.0). Patients were divided into two groups (high\_ *NOP56* versus low\_ *NOP56*) based on the optimal cutoff value of *NOP56* transcripts across all patients to plot the Kaplan–Meier survival curves.

For correlative analysis of *NOP56* expression with sensitivity ( $IC_{50}$ ) to mTOR inhibitors, gene expression data and drug response profiles were downloaded from Cancer Cell Line Encyclopedia (CCLE) and Genomics of Drug Sensitivity in Cancer (GDSC) databases, respectively. Correlation analysis was performed using R software (version 3.6.0).

### Statistical analysis

Statistical analyses were performed using GraphPad Prism 7.01 (GraphPad Software Inc., San Diego, CA, USA) unless otherwise indicated. In all studies, data represent biological replicates (n) and are depicted as mean values  $\pm$  SD or mean values  $\pm$  SEM as indicated in the figure legends. In all analyses, *P* values less than 0.05 were considered statistically significant. For the survival analysis, patients were grouped by gene expression, where ‘high’ and ‘low’ expression groups were stratified by the optimal cut-off value.

## Results

### **NOP56 confers a metabolic dependency by regulating ROS homeostasis in *KRAS*-mutant lung cancer**

To identify therapeutic vulnerabilities in *KRAS*-mutant cancers, we performed integrated analysis of shRNA- and CRISPR-based functional genomics of previously published studies [12, 16, 26]. To minimize lineage-specific effects, we analyzed whole-genome dropout screen dataset in *KRAS*-mutant lung (H460, H2122), colon (DLD-1), acute promyelocytic leukemia (NB4) and acute myeloid leukemia (SKM-1) cancer cells, which identified 21 common genes whose loss of function is synthetic lethal with mutant *KRAS* alleles in distinct cancer lineages (Fig. 1A; Table S4). The protein products of these genes fall into several functional categories, with FBL, *NOP56*, *PLK1* and *XPO1* as a core set based on their interaction network (Fig. 1B). Remarkably, *PLK1* and *XPO1* have been reported to be selectively required for *KRAS*-mutant cancers by counteracting mitotic and nuclear export stress associated with *KRAS*-induced tumorigenesis [12, 16], and our recent study has implicated *PLK1* in metabolic stress response of *KRAS*-mutant cancers [14]. *FBL* has also been assigned as a promising target in cancers [34, 35], suggesting the power of functional genomics in identifying oncogene-specific vulnerabilities and the accountability of our analyses. In the present study, we investigated the function of *NOP56* in *KRAS*-mutant cancers.

Our investigations began with *NOP56* knockdown using small interfering RNAs (siRNAs), which revealed that downregulation of *NOP56* significantly inhibited the proliferation of numerous *KRAS*-mutant lung (H358, H460, A549, PF563, PF139), pancreatic (MIAPaCa, HPAF-II) and colon (HCT-116, DLD-1) cancer cells, which differ not only in tumor lineages and histological subtypes but also in *KRAS* mutations, e.g., G12C, G12D, Q61H, etc. (Fig. S1A, B; Table S1). Notably, *NOP56* silencing also inhibited *NRAS*-mutant lung cancer H1299 cells, although the effects on *EGFR*-mutant (EBC-1) or *FGFR1*-amplified (H520) lung cancer cells were negligible (Fig. S1A, B). Supporting these observations, *KRAS*-mutant lung, pancreatic and colon cancer showed significantly higher expression of *NOP56* than *KRAS*-WT tumors (Fig. 1C) and patients with *KRAS*-mutant lung adenocarcinoma, pancreatic and colon cancer characterized by a higher *NOP56* level are associated with significantly shorter survival (Fig. 1D). In contrast, *NOP56* expression is not a prognostic marker for *KRAS*-mutant lung, pancreatic and colon cancers (Fig. S1C). These results indicate a unique function for *NOP56* in *KRAS*-mutant cancers.

To explore *NOP56* functions in *KRAS*-mutant malignancies, we profiled the transcriptomic gene expression data of a previous study [36], whereby *NOP56* in *KRAS*-mutant colon cancer cells (SW480) was silenced by siRNAs. Our analysis revealed that high expression of *NOP56* was positively correlated with the gene signature of *KRAS* signaling (Fig. S1D), in line with the above results (Fig. 1A–D; Fig. S1A, B), and that, importantly, siRNA-mediated *NOP56* knockdown led to significant enrichment of the gene sets involved in ROS pathway (consisting of 49 genes upregulated by ROS) and oxidative phosphorylation (a set of 200 genes encoding proteins involved in oxidative phosphorylation), the latter representing a major source of ROS production (Fig. 1E), suggesting a possible role for *NOP56* in the suppression of metabolic ROS that is critical for *KRAS*-induced tumorigenesis [27–30]. Supporting this notion, *NOP56* knockdown (KD) by siRNAs significantly upregulated ROS in H358 and H460 cells, and  $H_2O_2$  treatment, which elevated the already high level of oxidative stress, provoked significantly greater apoptosis in *NOP56* KD H358 and H460 cells than the control counterparts (Fig. 1F, G). These results uncover *NOP56* as a metabolic dependency in *KRAS*-mutant cancer by exerting a previously unrecognized role in the surveillance of oxidative stress.

### **NOP56 suppression evokes IRE1 $\alpha$ -mediated UPR to mitigate oxidative stress**

Next, we investigated the mechanism that *KRAS*-mutant cancer cells utilize to orchestrate cytotoxic ROS upon

NOP56 depletion. GSEA of transcriptomic dataset [36] revealed that *NOP56* knockdown significantly enriched the genes involved in the unfolded protein response/UPR (a set of 113 genes upregulated during UPR) in *KRAS*-mutant cancer cells (Fig. 2A), suggesting that tumor cells might engage the UPR to protect from *NOP56* KD-induced surge of cytotoxic ROS. To test this possibility, we knocked down *NOP56* in *KRAS*-mutant lung cancer cells (H358, H460) by using short-hairpin RNAs (shRNA) (Fig. S2A, B). In contrast to the results from siRNA-mediated acute depletion, stable expression of two independent shRNAs showed negligible effects on H358 and H460 proliferation (Fig. S2C, D), which may be due to the activation of compensatory mechanisms. Importantly, several UPR genes, in particular *ERN1* and *HSPA5* encoding the ER stress sensor IRE1 $\alpha$  and the chaperon protein BiP, respectively, were markedly upregulated in *NOP56*-depleted H358 and H460 cells (Fig. 2B). Western blot confirmed the increase of BiP, IRE1 $\alpha$ , XBP-1s (IRE1 $\alpha$  effector) and of the master UPR transcription factor HSF-1 (heat shock factor 1) and PDI (protein disulfide isomerase), an important ER chaperone induced during ER stress by carrying out a redox reaction and responsible for the formation of disulfide bonds in proteins (Fig. 2C). Notably, p38 MAPK, a key stress-responsive kinase and an UPR effector [37], was highly phosphorylated (activated) in *NOP56*-depleted H358 cells (Fig. 2C). Moreover, IRE1 $\alpha$  KD blunted p-p38, p-AKT (T308), p-MNK1, p-eIF4E and p-S6 in *NOP56*-depleted H358 cells, indicating that IRE1 $\alpha$ -mediated UPR acts upstream of p38 signaling (Fig. 2D).

Importantly, genetic (siRNA) and pharmacological (4 $\mu$ 8C, an inhibitor of IRE1 $\alpha$ ) inhibition of IRE1 $\alpha$  preferentially impaired *NOP56* KD H358 and H460 cells, manifested by significantly greater proliferative inhibition

and apoptotic induction in these cells than in control cells (Fig. 2E, F; Fig. S2E, F). Importantly, the increase of IRE1 $\alpha$  KD-induced apoptotic cell death was paralleled by ROS upregulation, and addition of NAC, an ROS scavenger largely dampened IRE1 $\alpha$  KD-induced apoptosis (Fig. 2F, G), supporting a role for the UPR in response to oxidative stress. Similarly, genetic and pharmacological inhibition (with KRIBB11) of HSF1 suppressed the proliferation and evoked apoptotic cell death to a markedly greater extent in *NOP56* KD H358 cells than in control cells (Fig. 2H–J).

The outcome of UPR ranges from adaptation to apoptosis [38] and, as such, perturbations of ER homeostasis in cells with an already high level of ER stress, e.g., treatment with bortezomib and tunicamycin that induce persistent ER stress by targeting the 26S proteasome and the ER chaperone BiP, respectively, evoke programmed cell death [38, 39]. Indeed, *NOP56* KD H358 and H460 cells with high basal levels of ROS are highly susceptible to bortezomib and Tunicamycin compared to control cells (Fig. 2K, L).

Thus, targeting *NOP56* disrupts ROS homeostasis and induces IRE1 $\alpha$ -mediated UPR in *KRAS*-mutant lung cancer cells.

#### IRE1 $\alpha$ -mediated UPR fuels mTOR signaling via p38 MAPK

To identify cellular processes that may present therapeutic vulnerabilities in *NOP56* KD cells, we performed synthetic lethal chemical screens with small-molecule drugs ( $n=22$ ) that interrogate various oncogenic pathways, with the ER stress inducers (bortezomib and HA15) included as positive controls (Table S2). Our screens showed that, except for bortezomib and HA15, LY294002, AZD5363, and rapamycin, inhibitors of the PI3K/AKT/mTOR pathway, preferentially suppressed

(See figure on next page.)

**Fig. 2** *NOP56* depletion evokes IRE1 $\alpha$ -mediated UPR. **A**, *NOP56* depletion led to significant enrichment of the UPR gene signature in *KRAS*-mutant cancer cells. GSEA was based on the GEO dataset GSE15212. **B**, Transcriptional quantification (qRT-PCR) of UPR genes in H358 and H460 cells expressing control (sh Scram) or *NOP56*-specific shRNA (sh *NOP56a*). **C**, Immunoblots of H358 and H460 cells expressing scrambled control or *NOP56*-specific shRNAs. **D**, H358 cells expressing scrambled control or *NOP56*-specific shRNAs were transfected with IRE1 $\alpha$ -specific or control siRNAs for 72 h before immunoblotting. **E**, Clonogenic assay of H460 and H358 cells expressing scrambled control or *NOP56*-specific shRNAs after treated with indicated doses of 4 $\mu$ 8C (IRE1 $\alpha$  inhibitor). Representative images are shown. **F**, H358 cells expressing scrambled control or *NOP56*-specific shRNAs were transfected with IRE1 $\alpha$ -specific or control siRNAs for 72 h, in the presence or absence of NAC (2.5 mM) before apoptosis assay. Data are presented as mean  $\pm$  SD ( $n=3$ ). \*\*\* $P<0.001$ , \*\*\*\* $P<0.0001$  and ns  $P>0.05$  by two-way ANOVA with Tukey's multiple comparisons test. **G**, H358 cells expressing scrambled control or *NOP56*-specific shRNAs were transfected with IRE1 $\alpha$ -specific or control siRNAs for 72 h, in the presence or absence of NAC (2.5 mM). Cells were then washed, incubated with H2DCFDA for 30 min, and analyzed by flow cytometry. Quantification of relative ROS levels was shown in the right. Data are presented as mean  $\pm$  SD ( $n=3$ ). \*\*\* $P<0.001$ , \*\*\*\* $P<0.0001$  and ns  $P>0.05$  by two-way ANOVA with Tukey's multiple comparisons test. **H**, H358 cells expressing scrambled control or *NOP56*-specific shRNAs were transfected with HSF1-specific or control siRNAs for 72 h before apoptotic assay. **I**, H358 cells expressing scrambled control or *NOP56*-specific shRNAs were transfected with HSF1-specific or control siRNAs for 72 h before immunoblot analysis. Data are presented as mean  $\pm$  SD ( $n=3$ ). \*\*\* $P<0.001$ , \*\*\*\* $P<0.0001$  and ns  $P>0.05$  by two-way ANOVA with Tukey's multiple comparisons test. **J**, Clonogenic assay of H460 and H358 cells expressing scrambled control or *NOP56*-specific shRNAs after treated with the indicated doses of KRIBB11 (HSF1 inhibitor). Representative images are shown. **K, L**, Clonogenic assay of H460 and H358 cells expressing scrambled control or *NOP56*-specific shRNAs after treated with the indicated doses of the ER stress inducer bortezomib (K) or tunicamycin (L). Representative images are shown



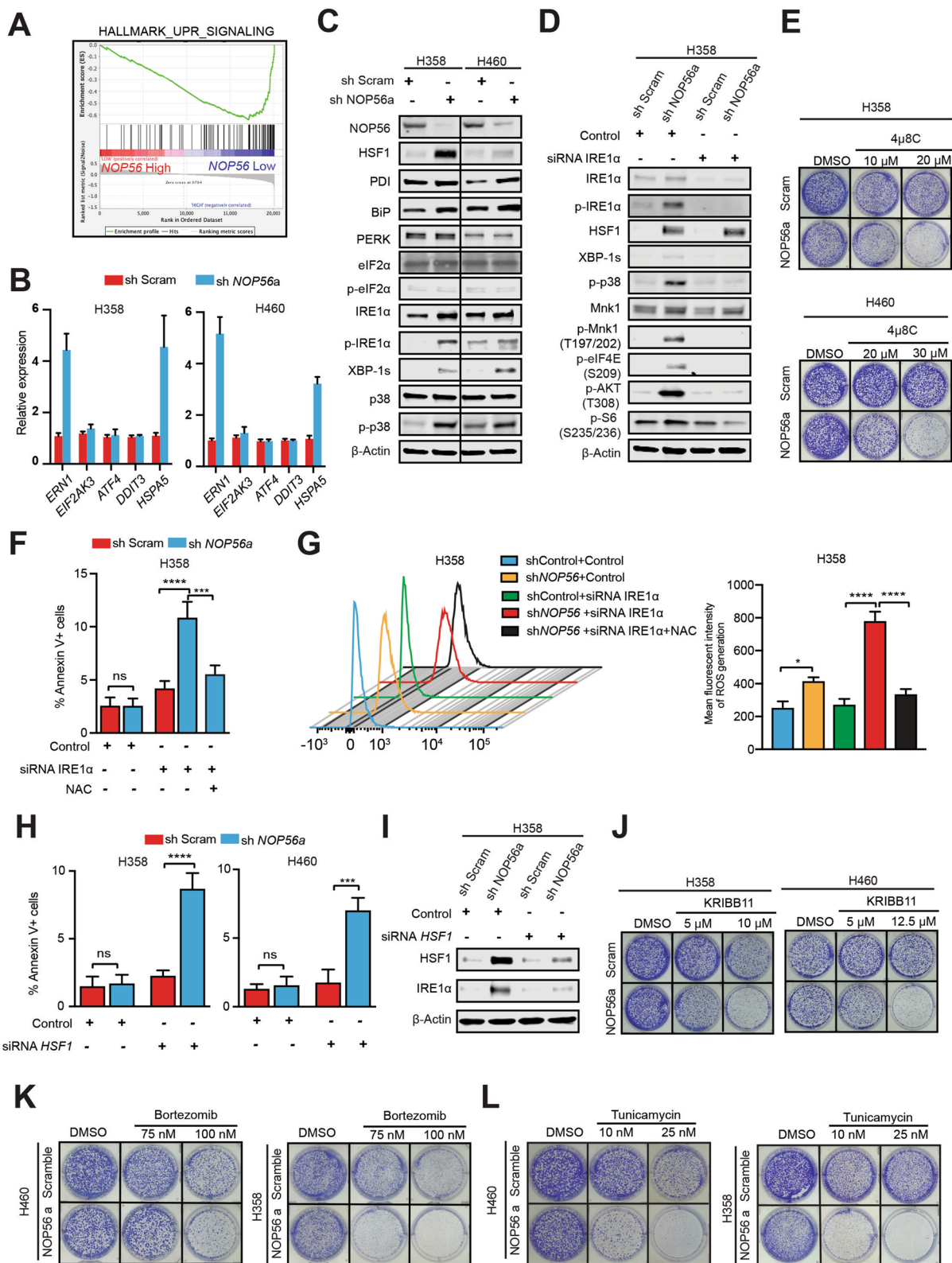


**Fig. 2** (See legend on previous page.)



the viability of *NOP56* KD cells, gauged by their  $IC_{50}$  decrease in *NOP56* KD H358 and H460 cells versus control cells (Fig. 3A; Fig. S3A). The greatest change in sensitivity was conferred by rapamycin, which was 0.7  $\mu$ M and 1.0  $\mu$ M in H358\_shNOP56a and H358\_shNOP56b but 12.0  $\mu$ M in H358\_Scr cells, with a selectivity index ( $IC_{50}$  in control cells /  $IC_{50}$  in *NOP56* KD cells) of 17- and 12-fold, respectively (Fig. 3A; Fig. S3A). These observations were validated by independent assays, in which *NOP56* KD sensitized H358 and H460 cells to PI3K/AKT inhibitors (LY294002, AZD5363), anti-mTOR drugs (rapamycin, everolimus), and ER stress inducers (bortezomib and HA15) (Fig. 3B,C; Fig. S3B,C). Importantly, CRISPR/Cas9-mediated knockout of *NOP56* dramatically increased the sensitivity of *KRAS*-mutant (H358, H460) but not of wild-type (H520, H1703) lung cancer cells to rapamycin (Fig. S3D, E).

Moreover, examining gene expression data of *KRAS*-mutant cancer cells [36] revealed that *NOP56* silencing significantly enriched the mTOR gene signature (Fig. 3D). Mining TCGA and Genomics of Drug Sensitivity in Cancer (GDSC) databases showed that *NOP56* expression is negatively correlated with that of mTOR pathway genes in patients with *KRAS*-mutant lung adenocarcinomas (Fig. 3E) and that *NOP56* mRNA levels are a predictive marker of sensitivity ( $IC_{50}$ ) to rapamycin in *KRAS*-mutant cancer cell lines but not in *KRAS*-wild-type cancer cells (Fig. 3F). These data support our in vitro results (Fig. 3A-C; Fig. S3A-C) and further suggest a reciprocal interplay between *NOP56* and mTOR signaling.

Indeed, siRNA-mediated *NOP56* KD, which slightly increased ribonucleolar proteins (e.g., *NOP58*, *FBL*), markedly induced AKT/mTOR (p-AKT, p-mTOR, pS6), translation initiation (p-eIF4E) and the stress-responsive p38 MAPK in H358 cells in a time-dependent manner (Fig. 3G), as did shRNA-mediated stable *NOP56*

KD in H358 and H460 cells, but not in *KRAS*-WT lung cancer H1703 cells (Fig. 3H; Fig. S3G). Importantly, *NOP56* KD sensitized *KRAS*-mutant lung (A549), colon (HCT-116, DLD-1, and LS174T), pancreatic (MIAPaCa, HPAF-II) and primary *KRAS*-mutant lung cancer cells (PF563, PF139) to rapamycin, as well as *NRAS*-mutant lung cancer H1299 cells but not *KRAS*-wild-type H2405 (BRAF-mutant), EBC-1 (EGFR-mutant), H1993 (MET amplification) and H520 (FGFR1 amplification) cells (Fig. S3H, I). These results reinforce the notion that *NOP56* plays a unique role in *KRAS*-mutant cancer.

Our results demonstrated that *NOP56* and the IRE1 $\alpha$ -mediated UPR act upstream of p38 and mTOR signaling (Fig. 2C, D; Fig. 3G), suggesting a signaling cascade from the UPR to mTOR via p38 MAPK. To confirm this, we targeted p38 with the specific inhibitor SB203580, which, as expected, barely affected the upstream IRE1 $\alpha$ -dependent UPR (p-IRE1 $\alpha$ , XBP-1s), but strikingly dampened the MNK-eIF4E axis and mTOR signaling (p-AKT, p-S6) in H358 cells (Fig. 3I). Importantly, SB203580 exposure not only decreased activity of the mTOR pathway but also increased PARP expression and promoted PARP cleavage (Fig. 3I), concurrent with substantially elevated cytotoxicity on *NOP56* KD H460 and H358 cells compared to that on control cells (Fig. 3J). Together, these results unravel a signaling cascade from the IRE1 $\alpha$ -mediated UPR to p38 MAPK and to mTOR signaling in *KRAS*-mutant lung cancer upon *NOP56* suppression.

### Synthetic lethality by targeting *NOP56* and mTOR in *KRAS*-mutant lung cancer

Our findings that *NOP56* KD cells are exposed to higher levels of metabolic ROS and display a greater dependency on UPR-activated mTOR signaling suggest a synthetic lethal vulnerability in *KRAS*-mutant cancer (Figs. 1, 2, 3). To test this hypothesis, we treated *NOP56* KD H358

(See figure on next page.)

**Fig. 3** IRE1 $\alpha$ -mediated UPR fuels mTOR signaling via p38 MAPK. **A**, H358 cells expressing scrambled control or *NOP56*-specific shRNAs were treated with different inhibitors, with bar graphs illustrating sensitivity increase after *NOP56* KD. Fold changes of  $IC_{50}$  values were presented as  $IC_{50}$  of rapamycin in H358 cells expressing scrambled shRNA (sh\_Scrambled) compared to that in H358 cells expressing *NOP56*-targeted shRNAs (shNOP56 a/b). Data presented as mean ( $n = 2$ ). **B**, Clonogenic assay of H358 and H460 cells expressing control shRNA (sh\_Scr) or *NOP56*-specific shRNAs (sh-a, sh-b) after treatment with indicated doses of rapamycin or everolimus. Representative images are shown. The heatmap (right) indicates the percentage of viable cells after the treatment, based on quantification of clonogenic results (left). Data are presented as mean  $\pm$  SD ( $n = 3$ ). **C**, Growth inhibition of H358 and H460 cells expressing *NOP56*-specific shRNAs (sh NOP56a, sh NOP56b) or control shRNAs (sh Scram) after treated for 72 h with the mTOR inhibitors (rapamycin, everolimus). Data are presented as mean  $\pm$  SD ( $n = 3$ ). **D**, *NOP56* silencing significantly enriched the mTOR gene signature in *KRAS*-mutant cancer cells. GSEA was performed based on the GEO dataset GSE15212. **E**, Negative correlation of *NOP56* mRNA levels with mTOR gene signature (mTOR pathway score) as determined in a TCGA cohort of patients with *KRAS*-mutant lung adenocarcinoma. Pearson and Spearman coefficient, as well as the significance ( $p$ -value), were determined using R software (Cor.test function). **F**, *NOP56* expression is a predictive marker of sensitivity ( $IC_{50}$ ) to rapamycin in *KRAS*-mutant cancer cell lines ( $n = 18$ ) but not in *KRAS*-wild-type cancer cell lines ( $n = 82$ ). Drug response profiles were downloaded from the GDSC (Genomics of Drug Sensitivity in Cancer) database. **G**, Immunoblots of H358 cells after transfection with scramble control siRNAs (si-Control) for 72 h (–) or *NOP56*-specific siRNAs (si-NOP56) for different time points (24 h, 48 h, 72 h and 96 h). **H**, Immunoblots of H358 and H460 cells expressing scrambled control or *NOP56*-specific shRNAs. **I**, Immunoblots of H358 cells expressing scramble control or the *NOP56*-specific shRNAs after treated with the p38 inhibitor SB203580 (5  $\mu$ M) for 24 h. **J**, Clonogenic assay of H460 and H358 cells expressing control or *NOP56*-specific shRNAs after treated with the p38 inhibitor SB203580. Representative images are shown

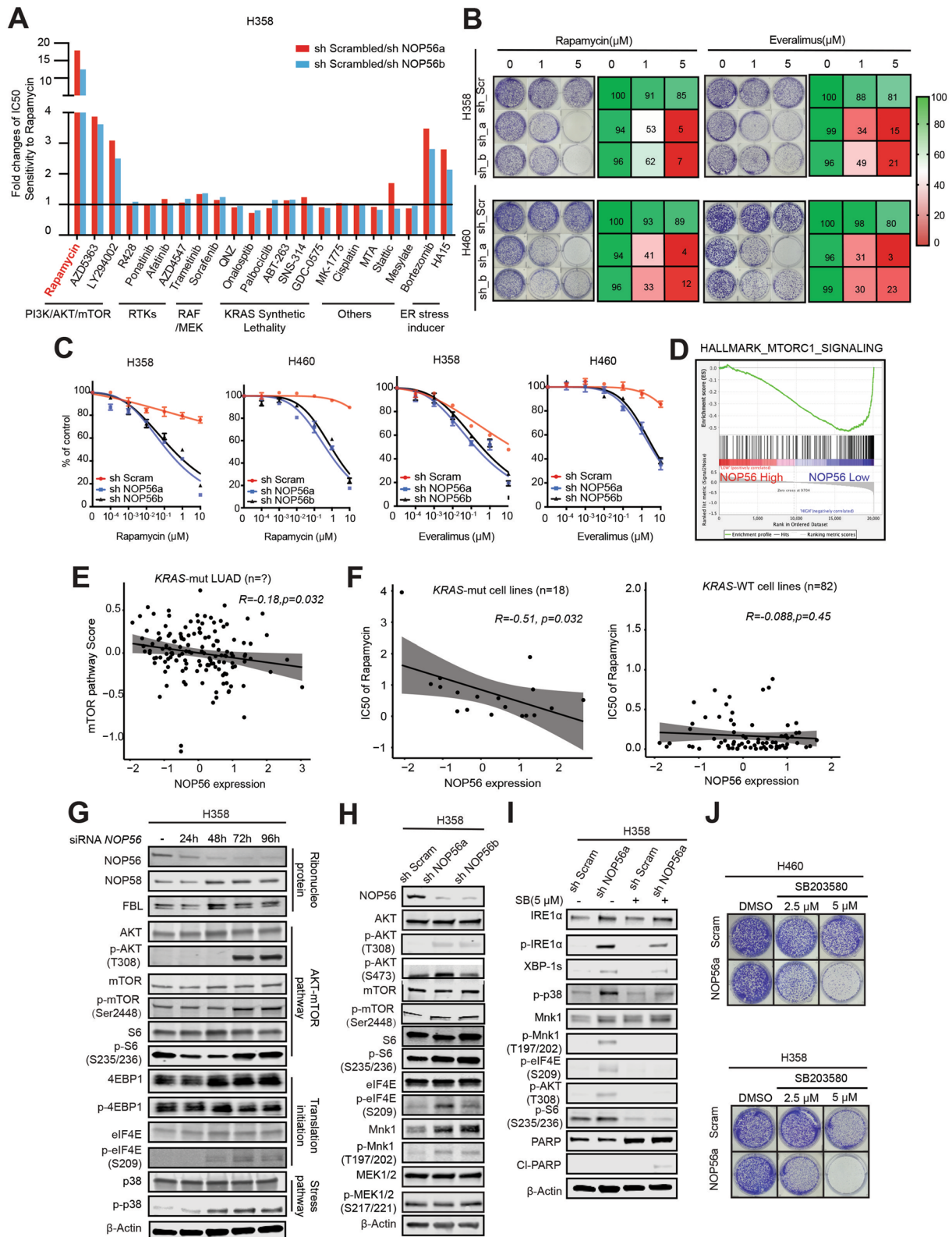


**Fig. 3** (See legend on previous page.)

and control cells with rapamycin, which, as expected, decreased mTOR effectors (e.g., p-S6, p-eIF4E) (Fig. 4A) that were the otherwise adaptively upregulated upon NOP56 depletion (Fig. 3G, H). Strikingly, rapamycin induced PARP cleavage (CI-PARP) in *NOP56* KD H358 but not in control cells (Fig. 4A), indicating that concomitant targeting of NOP56 and mTOR caused synthetic lethality. Similar results were observed in *NOP56* KD H358 cells that were treated with the AKT inhibitor AZD5363 (Fig. S4A, B). Knockdown of Raptor and Rictor, key components of the mTORC1 and mTORC2, respectively, significantly suppressed the viability of *NOP56* KD H358 cells despite to differential extent (Fig. S4C, D). Moreover, whereas individual S6 and eIF4E only partly contributed to the viability of *NOP56* KD H358 cells, concomitant inhibition of S6 (siRNA) and eIF4E (siRNA and Briciclib, an eIF4E inhibitor) led to significantly enhanced anti-proliferative effect (Fig. 4B-G; Fig. S4E) and largely recapitulated the impact seen by mTOR inhibition with rapamycin (Fig. 4A, Fig. S4F), gauged by the extent to which apoptotic markers (CI-PARP) were induced in *NOP56* KD H358 cells (Fig. 4F). These results interrogate an important role for mTOR to relay the IRE1 $\alpha$ -mediated UPR signaling in *NOP56*-depleted *KRAS*-mutant lung cancer.

The UPR is a double-edged sword, as its outcome flips from adaption to apoptosis when malfunctioning UPR, a condition at which stress stimuli are overwhelming or the UPR signal cannot be properly relayed [38, 39]. We thus assumed that the observed synthetic lethality of *NOP56* and mTOR inhibition might be enabled due to malfunctioning UPR. Indeed, co-targeting *NOP56* and mTOR resulted in synergistic effects that not only increased the expression of IRE1 $\alpha$  and p-IRE1 $\alpha$ , indicative of hyperactive UPR signals, but also upregulated p-JNK, FOXO3A and BIM, a BH3 only protein and key mediator of apoptotic balance (Fig. 4H). Consistent with their pro-apoptotic roles, this increase of the JNK-FOXO3A-BIM axis was accompanied by PARP cleavage (CI-PARP) and

significantly greater apoptotic cell death in *NOP56* KD H358 and H460 cells compared to control cells (Fig. 4H, I). Importantly, IRE1 $\alpha$  KD (siRNA) precluded the cytotoxicity of combined *NOP56* and mTOR inhibition, evidenced by decreased levels of p-JNK, FOXO3a, BIM, CI-PARP and of apoptotic populations in *NOP56* KD H358 and H460 treated with rapamycin (Fig. 4H, I). Similarly, inhibiting JNK activity by the inhibitor SP600125 dampened the efficacy of rapamycin in *NOP56* KD H358 and H460 cells (Fig. 4J). Thus, IRE1 $\alpha$ -mediated UPR activates mTOR, which provides a survival signal for *NOP56* KD *KRAS*-mutant cancer cells; conversely, mTOR inhibition leads to overwhelmed UPR and promotes apoptotic cell death by activating the JNK-FOXO3A-BIM axis (Fig. 4K).

#### **NOP56 and mTOR converge on a metabolic liability in *KRAS*-mutant lung cancer**

Next, we asked if the synthetic lethality of co-targeting *NOP56* and mTOR is a result of unresolvable metabolic stress. Indeed, rapamycin sensitivity of *NOP56* KD H358 and H460 cells was highly correlated with ROS levels (Fig. 5A, B), and ROS scavenge by NAC significantly compromised the cytotoxicity of rapamycin (Fig. 5B), highlighting a causative link between ROS and rapamycin-induced apoptosis in *NOP56* KD cells.

These results uncover a novel homeostatic mechanism of metabolic stress mediated by *NOP56* and validate an unexpected synthetic lethality by targeting *NOP56* and mTOR that aggregate a metabolic liability in *KRAS*-mutant lung cancer (Fig. 5C).

#### **NOP56 downregulation plus rapamycin potently suppresses in vivo tumor growth of *KRAS*-mutant lung cancer**

Finally, we investigated in vivo efficacy of co-targeting *NOP56* and mTOR. In a xenograft model from *KRAS*-mutant H460 cells, *NOP56* knockdown (sh*NOP56*) only mildly inhibited tumor growth compared to control

(See figure on next page.)

**Fig. 4** Synthetic lethality by targeting *NOP56* and mTOR in *KRAS*-mutant lung cancer cells. **A**, Immunoblots of H358 cells expressing scramble control or *NOP56*-specific shRNAs after treated with rapamycin (1  $\mu$ M) for 24 h. **B-G** H358 cells expressing scramble control or sh*NOP56*-specific shRNAs were transfected with control siRNAs or the indicated siRNAs specifically targeting S6, eIF4E, alone and in combination. The cells were then subjected to immunoblots (B, D, F) and viability assay (C, E, G) 72 h post-transfection. Data are presented as mean  $\pm$  SD ( $n = 3$ ). **H**, H358 cells expressing scrambled control or *NOP56*-specific shRNAs were transfected with *IRE1 $\alpha$* -specific or control siRNAs for 48 h, followed by treatment with rapamycin (1  $\mu$ M) for 24 h before immunoblotting. **I**, H358 cells expressing control or *NOP56*-specific shRNAs were transfected with *IRE1 $\alpha$* -specific or control siRNAs for 24 h, followed by treatment with rapamycin (5  $\mu$ M) for 72 h before apoptosis assay. Data are presented as mean  $\pm$  SD ( $n = 3$ ). \* $p < 0.05$ , \*\*\* $p < 0.001$  and \*\*\*\* $p < 0.0001$  by two-way ANOVA with Tukey's multiple comparisons test. **J**, H358 cells expressing control or *NOP56*-specific shRNAs were preincubated overnight with vehicle (DMSO) or the JNK inhibitor SP600125, followed by treatment with rapamycin for 72 h before apoptosis assay. Data are presented as mean  $\pm$  SD ( $n = 3$ ). \*\* $p < 0.01$ , \*\*\* $p < 0.001$  and ns  $P > 0.05$  by two-way ANOVA with Tukey's multiple comparisons test. **K**, Proposed model of cellular gauge for IRE1 $\alpha$ -regulated UPR. In *KRAS*-mutant cancer cells, intact *NOP56* keeps ROS in check so that IRE1 $\alpha$ -regulated UPR is minimal (basal level; left). Intermediate levels of IRE1 $\alpha$ -regulated UPR ensue from *NOP56* depletion, which activates p38-AKT/mTOR and promotes cell survival (middle). At "dangerous" level of ROS, IRE1 $\alpha$ -regulated UPR initiates JNK-dependent apoptosis (right)

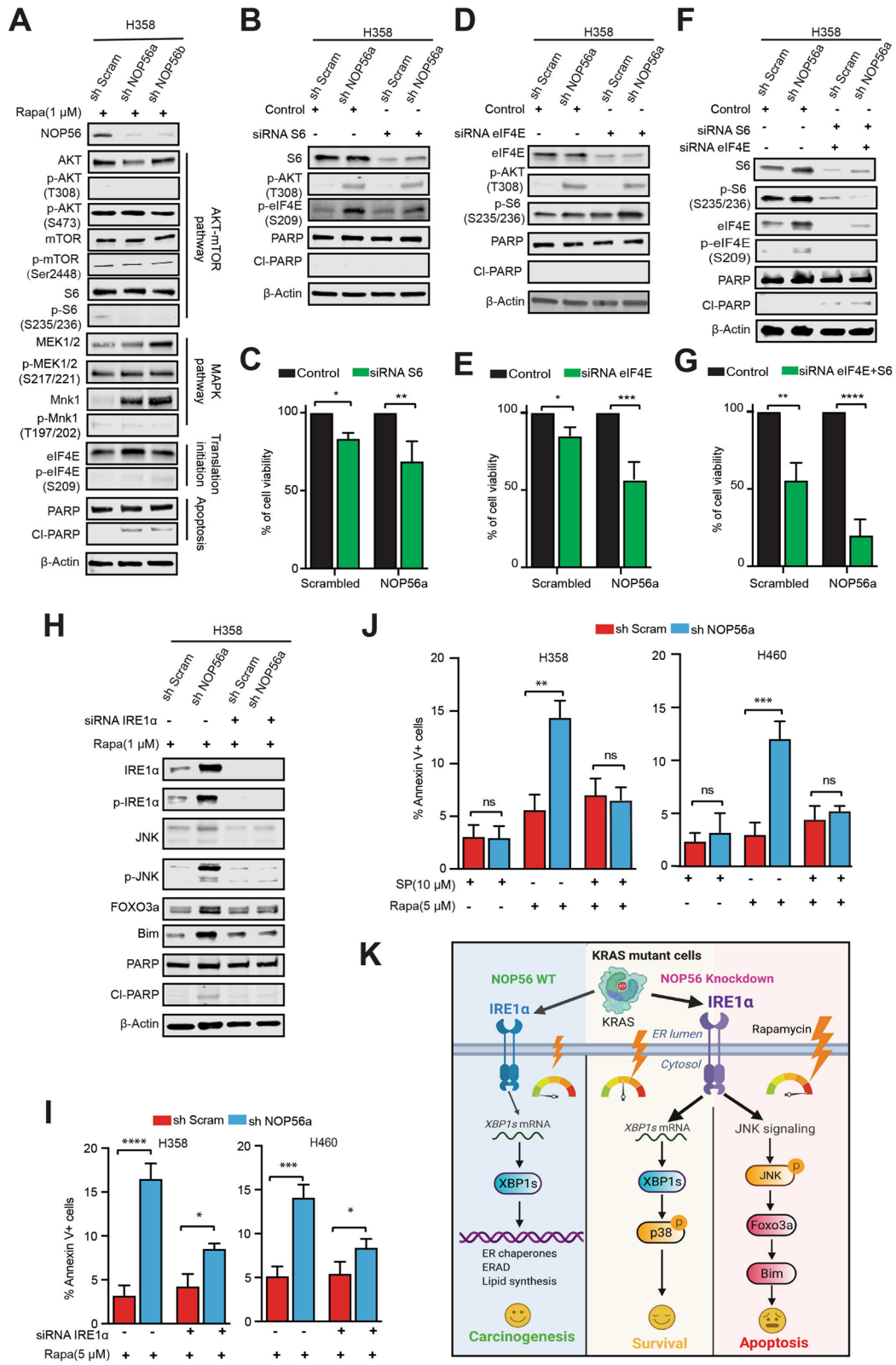
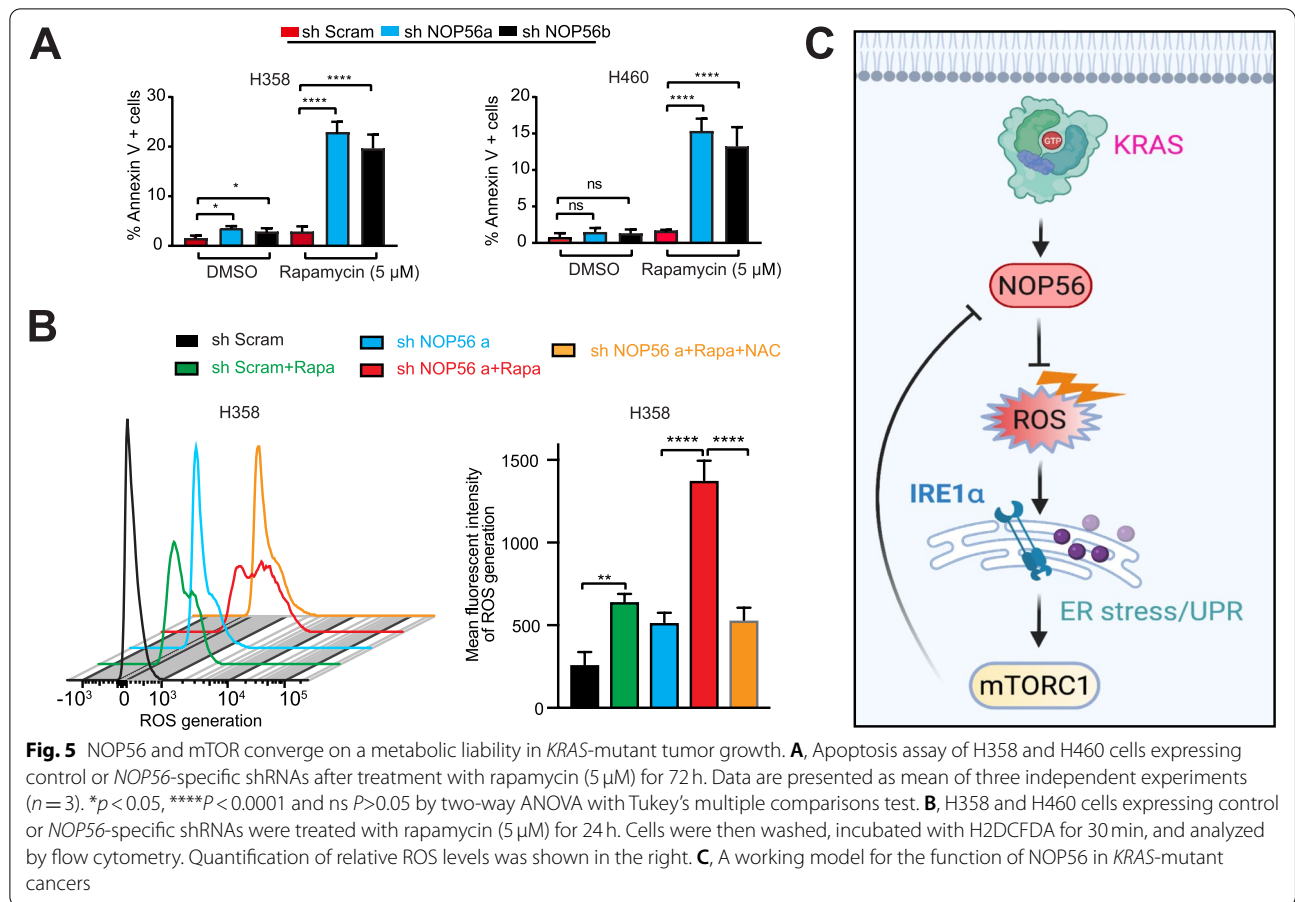


**Fig. 4** (See legend on previous page.)





shRNA (shScrambled), as did rapamycin (Fig. 6A). However, the outcome of concomitant targeting of *NOP56* and mTOR (sh*NOP56* plus rapamycin) was superior to that achieved by sh*NOP56* or rapamycin alone, leading to far more effective and potent suppression of xenograft tumor growth (Fig. 6A, B). Residual tumors (after 3-week treatment) from the combination group (sh*NOP56* plus rapamycin) were typically tiny and significantly differed from those of the other treatment groups (Fig. 6C). Immunohistochemical

(IHC) analysis revealed that the anti-tumor efficacy of combined treatment with sh*NOP56* and rapamycin was paralleled by marked decrease of mTOR activity (p-AKT, p-mTOR, p-S6) and increase in apoptosis (Caspase-3) in the residual tumors (Fig. S5A).

Similar results were obtained from H358 xenografts (Fig. 6D, E) and a patient-derived xenograft (PDX) model established from the primary *KRAS*-mutant PF139 cells (Fig. 6F-I). In both models, *NOP56* KD sensitized H358 and PF139 xenograft tumors to rapamycin, leading to

(See figure on next page.)

**Fig. 6** *NOP56* knockdown plus rapamycin inhibits *KRAS*-mutant tumor growth. **A**, Growth curve of xenograft tumors derived from H460 cells expressing either a control or an shRNA against *NOP56* (sh*NOP56a*). Rapamycin (0.1 mg/kg) was administered i.p. for 3 weeks (5 days/week). Data are shown as mean  $\pm$  SD. \*\*\* $P < 0.001$ , \* $P < 0.05$  and ns ( $P > 0.05$ ) by two-way ANOVA with Tukey's multiple comparisons test. **B**, Relative tumor volume of H460 xenograft tumors after the treatment for 3 weeks. **C**, Weights of H460 xenograft tumors after the treatment for 3 weeks. \*\*\* $P < 0.001$  by one-way ANOVA with Tukey's multiple comparisons test. **D**, Growth curve of xenograft tumors derived from H358 cells expressing either a control or an shRNA against *NOP56* (sh*NOP56a*). \*\* $P < 0.01$  by two-way ANOVA with Tukey's multiple comparisons test. **E**, Kaplan-Meier survival curve of mice with H358 xenografts from the experiment in **D**. **F**, Growth curve of PDX tumors derived from primary *KRAS*-mutant PF139 lung cancer cells expressing either control or *NOP56*-specific shRNAs. Data are shown as mean  $\pm$  SD. \*\*\* $P < 0.001$  and \* $P < 0.05$  by two-way ANOVA with Tukey's multiple comparisons test. Immunoblots of PF139 cells expressing *NOP56*-specific or scrambled shRNAs was also shown. **G**, Relative tumor volume of PF139 xenografts after 3 weeks of treatment. **H**, Weights of PF139 xenograft tumors after treated for 3 weeks. \*\*\* $P < 0.001$ , \* $P < 0.05$  and ns  $P > 0.05$  by two-way ANOVA with Tukey's multiple comparisons test. **I**, H&E and IHC of p-AKT(T308), p-mTOR(S2448), p-S6(S235/236), Ki67 and Caspase-3) in PF139 xenograft tumors after the treatment. Scale bars 100  $\mu$ m

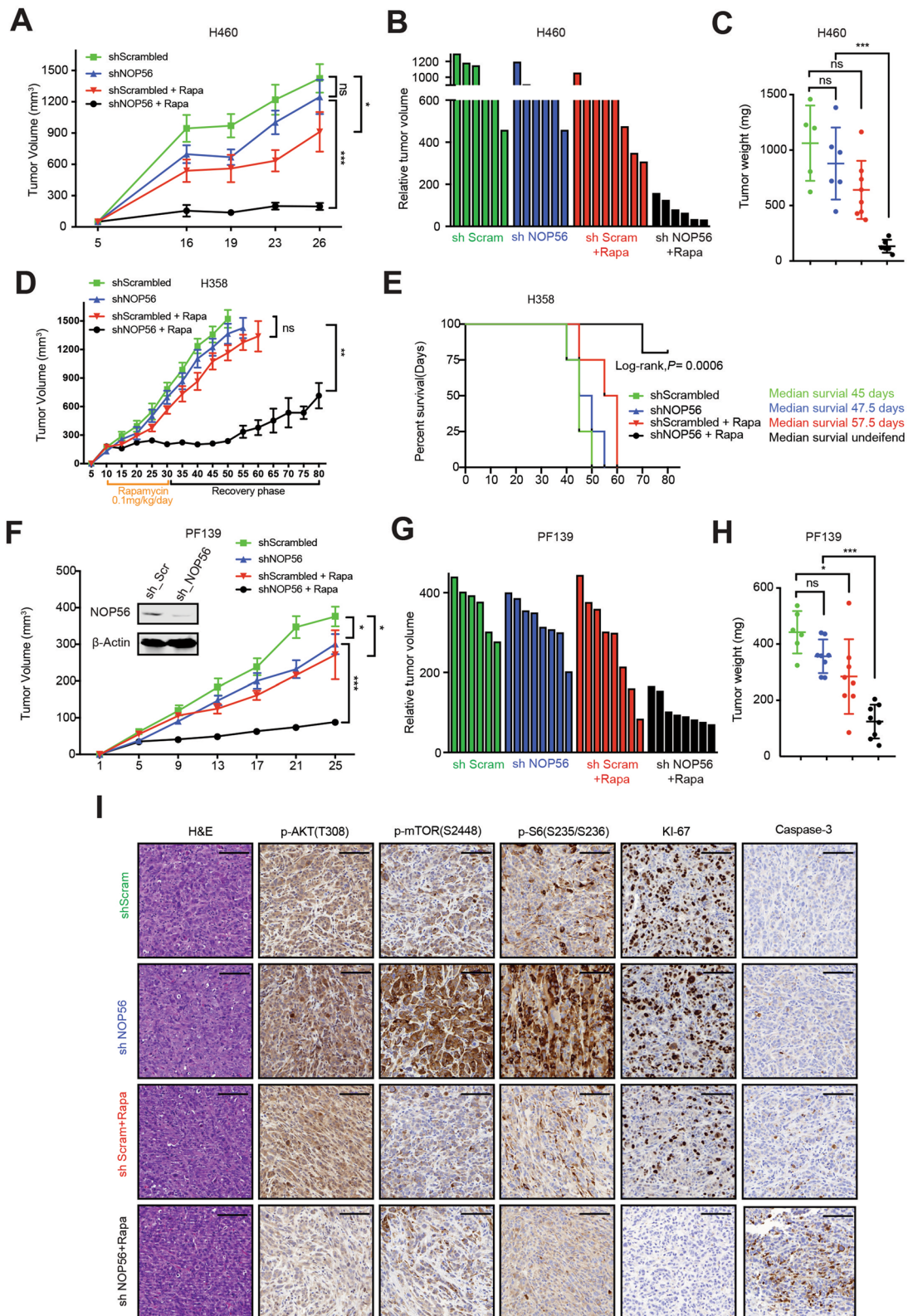


**Fig. 6** (See legend on previous page.)

potent suppression of tumor growth (Fig. 6D, F-H) and significant improvement of mouse survival (Fig. 6E). IHC of the PF139 residual tumors revealed that NOP56 depletion plus rapamycin strikingly suppressed tumor cell proliferation (Ki-67) and dampened mTOR activity (p-AKT, p-mTOR and p-S6), but increased Caspase-3 cleavage (Fig. 6I), which is consistent with the *in vitro* results (Figs. 4, 5) and our observations on H460 xenografts (Fig. S5A). Notably, rapamycin showed little beneficial effects in *NOP56* KD *KRAS* wild-type H1703 xenografts (Fig. S5B, C), which mirrors the *in vitro* data and reinforces the selective activity of co-targeting NOP56/mTOR in *KRAS*-mutant lung cancer.

Together, these results support a model that NOP56 downregulation induces a metabolic vulnerability to mTOR inhibition, which presents a new and rational strategy for treating *KRAS*-mutant lung cancer.

## Discussion

In the present study, we have uncovered a new and unanticipated mechanism by which NOP56 and mTOR signaling cooperate in metabolic stress response in *KRAS*-mutant lung cancer. We show that NOP56 suppresses ROS, and its depletion induces synthetic lethal susceptibility to inhibition of mTOR that is otherwise essential for counterbalance of the resurgence of cytotoxic ROS evoked by NOP56 downregulation. We also discover that mTOR activation is driven by IRE1 $\alpha$ -mediated UPR via p38 MAPK. These findings support a model that NOP56 plays a role in the surveillance of ROS homeostasis and suggest that concomitant blockage of NOP56 and mTOR signaling has the potential to selectively target *KRAS*-mutant lung cancer. As multiple mTOR inhibitors (e.g., rapamycin and everolimus) are clinically approved drugs, our observations have immediate translational significance.

Despite decades-long steady efforts, therapeutic targeting of *KRAS*-mutant cancers has remained an overarching challenge in clinical oncology [3]. A promising strategy to target *KRAS*-driven tumors is to exploit cancer cell vulnerabilities contextually co-opted by mutant *KRAS*, in light of the concept that mutant *KRAS* alter physiological biochemical networks and induces cellular stresses, rendering *KRAS*-mutant cancer particularly susceptible to inhibition of stress-remedy mechanisms [12–14]. Empowered by CRISPR- and shRNA-based functional genomics, a plethora of novel factors required for *KRAS*-mutant cancer cells have been identified [12–16, 26], although the long-sought-after universal synthetic lethal targets for *KRAS*-driven pan-cancers are still at large. By implementing integrated analysis of functional genomic datasets ( $n=5$ ) derived from shRNA- and CRISPR-based screens [12, 16, 26], we revealed

that NOP56 confers a metabolic requirement for *KRAS*-mutant cancer by regulating ROS homeostasis. A functional link between NOP56 and mutant *KRAS* is supported by a multitude of lines of evidence, i.e., the elevated expression of NOP56 in *KRAS*-mutant tumors, the prognostic significance of NOP56 expression in patients with *KRAS*-mutant but not wild-type cancers, and selective damage on *KRAS*-mutant cancer cells incurred by NOP56 downregulation.

Moreover, our results uncover a reciprocal interaction of NOP56 and mTOR signaling and suggest that combined inhibition of NOP56/mTOR is a rational strategy to combat *KRAS*-mutant cancer. Supporting our findings, mRNA levels of *NOP56* significantly correlate with that of mTOR pathway genes in *KRAS*-mutant cancer cells and lung adenocarcinomas, and *NOP56* expression is a predictive marker of sensitivity to mTOR inhibitors in *KRAS*-mutant but not *KRAS*-wild-type cancer cells. Importantly, *NOP56* knockdown sensitizes *KRAS*-mutant cancer cells to mTOR inhibitors *in vitro* and *in vivo*, which is not true for *KRAS*-wild-type tumor cells. Despite potential toxicological challenges as ribosome biogenesis is also an important physiological process, modulation of NOP56 activity may afford a therapeutic window for targeted inhibition of mTOR in *KRAS*-mutant cancers.

An increasingly growing body of evidence suggests that oncogenic *KRAS* signaling rewires metabolic pathways to meet the energetic and biosynthetic demands of cancer cells [27–30, 40]. In particular, increased ROS production, which has been shown to be functionally required for *KRAS*-mediated tumorigenicity [27, 28], is a key metabolic manifestation associated with *KRAS*-mutant cancer cells [27–30]. Since excess ROS is harmful, cancer cells must leverage ROS levels to favor tumor progression but prevent cell death [14, 27–30, 41]. Here, we reported, for the first time, a role for NOP56 in metabolic ROS response in *KRAS*-mutant lung cancer. NOP56 is a key component of box C/D snoRNPs that regulates ribosome assembly. This process has been shown to be deregulated in tumors with increased requirement for protein synthesis, providing cancer vulnerabilities for therapeutic avenues [21–24, 42–45]. Our results are also in line with previous studies reporting cancer subtype-specific alterations in ribosome assembly and biogenesis processes [44, 45]. In addition, recent evidence suggests that snoRNPs may also be involved in other processes independent of their functions in ribosome biogenesis [46]. Future studies will be necessary to clarify whether the newly identified metabolic role of NOP56 in *KRAS*-mutant cancer is related to its canonical role.

Our finding that IRE1 $\alpha$ -mediated UPR connects the NOP56 function in ROS scavenge with mTOR



signaling, a master regulator of cellular metabolism [47], provides mechanistic insights about the synthetic lethality of co-targeting NOP56 and mTOR, which is supported the observation that challenges to ribosome biogenesis result in acute loss of proteostasis [48]. IRE1 $\alpha$ -mediated UPR, whilst initially protective, turns to be pro-apoptotic if ROS-induced metabolic stress is prolonged and persists [38, 39]. We further reveal that the overwhelming metabolic stress incurred by NOP56 depletion and mTOR inhibition activates the JNK-BIM axis, a stress-responsive pathway that promotes cell-cycle arrest and apoptosis [37]. The observation that UPR is a key component of the homeostatic mechanism in response to ROS resurge evoked by NOP56 knockdown is consistent with the notion that UPR plays an important role in homeostasis regulation including ROS and that challenges to ribosome biogenesis result in acute loss of proteostasis [49]. As metabolic ROS is causally linked to mutant KRAS-induced tumorigenicity and requires homeostatic mechanisms to maintain ROS levels within a threshold favorable for tumor development [14, 27–30, 41], the identification of NOP56 and mTOR converging on a role as ROS scavengers reveals an unanticipated metabolic vulnerability in KRAS-mutant cancers.

## Conclusion

In summary, we have uncovered an unexpected role for NOP56 in the surveillance of metabolic ROS in KRAS-mutant lung cancer. We have also revealed a novel synthetic lethality between NOP56 depletion and mTOR inhibitors that occurs by impeding the homeostatic mechanism of ROS in KRAS-mutant cancer cells. Moreover, we have demonstrated that mTOR activation upon NOP56 depletion is driven by IRE1 $\alpha$ -mediated UPR. These results shed light on the mechanisms underlying KRAS-induced metabolic rewiring, reveals an unanticipated metabolic vulnerability in KRAS-mutant lung cancer, and suggest a new rationale for the treatment of the disease. Because KRAS alterations are implicated in a broad spectrum of human malignancies, our findings may also be applicable to other lineages of cancer with high frequencies of KRAS alterations.

## Abbreviations

GSEA: Gene Set Enrichment Analysis; IRE1 $\alpha$ : Inositol-requiring enzyme 1 $\alpha$ ; KRAS: Kirsten rat sarcoma viral oncogene homolog; mTOR: Mechanistic target of rapamycin; NOP56: Nucleolar protein 5A; PARP: Poly (ADP-ribose) polymerase; RNAi: RNA interference; ROS: Reactive oxygen species; TCGA: The Cancer Genome Atlas; UPR: Unfolded protein response.

## Supplementary Information

The online version contains supplementary material available at <https://doi.org/10.1186/s13046-022-02240-5>.

**Additional file 1: Figure S1.** NOP56 knockdown inhibits proliferation of KRAS-mutant cancer cells. **A**, Immunoblots of KRAS-mutant and KRAS-wild type cancer cells that were transfected with NOP56-specific siRNAs (si-NOP56) or scramble control siRNAs (si-Control). **B**, KRAS mutant and KRAS wild type cancer cells were transfected with control siRNAs or NOP56-specific siRNAs. Cell viability was determined 72 h post transfection. Data are presented as mean  $\pm$  SD ( $n = 3$ ). \* $p < 0.05$ , \*\* $p < 0.01$ , \*\*\* $p < 0.001$ , \*\*\*\* $p < 0.0001$  and ns  $P > 0.05$  by two-way ANOVA with Tukey's multiple comparisons test. **C**, NOP56 is not a biomarker of survival in patients with KRAS-wild-type lung adenocarcinoma (LC), pancreatic cancer (PC) and colon cancer (CC). Kaplan–Meier survival analyses of patient cohorts in TCGA were stratified by the optimal cut-off value of the mRNA level of NOP56. **D**, Gene set enrichment analysis (GSEA) of a TCGA cohort of patients with KRAS-mutant lung ( $n = 141$ ), pancreatic ( $n = 133$ ) and colon cancer ( $n = 170$ ). **Figure S2.** Stable expression of NOP56-specific shRNAs activates IRE1 $\alpha$ -mediated UPR. **A**, Immunoblots of H358 and H460 cells expressing scrambled control or NOP56 shRNAs. **B**, Immunofluorescence of H358 and H460 cells that express scrambled control or NOP56 shRNAs. The NOP56 signal is indicated by arrowheads. **C**, The cell viability curve of H358 and H460 cells expressing scramble control shRNA or the NOP56-targeted shRNAs was measured at the indicated time points. **D**, Clonogenic assay of H358 and H460 cells expressing scramble control or NOP56-targeted shRNAs. Quantification of clonogenic assay were shown underneath. Data are presented as mean  $\pm$  SD ( $n = 3$ ). **E**, Growth inhibition of H358 and H460 cells expressing control shRNA or NOP56-targeted shRNA (3000 cells/well) treated for 72 h with the indicated doses of an IRE1 $\alpha$  inhibitor (4 $\mu$ 8C). Data are presented as mean  $\pm$  SD ( $n = 3$ ). **F**, Apoptosis assay of H460 cells expressing scrambled control or NOP56-targeted shRNAs after transfection with IRE1 $\alpha$ -specific or control siRNAs for 72 h. Data are presented as mean  $\pm$  SD ( $n = 3$ ). \*\*\* $P < 0.001$  and ns  $P > 0.05$  by two-way ANOVA with Tukey's multiple comparisons test. **Figure S3.** NOP56 KD renders KRAS-mutant lung cancer cells susceptible to mTOR inhibition. **A**, Bar graphs illustrating the change of sensitivity to different inhibitors in H460 cells after NOP56 knockdown. Data are presented as IC<sub>50</sub> values of the indicated inhibitors in H460 cells expressing scramble control shRNAs compared to IC<sub>50</sub> in H460 cells expressing NOP56-targeted shRNAs. Data are shown as mean ( $n = 2$ ). **B**, Viability assay of H460 and H358 cells expressing control shRNA or NOP56-targeted shRNA (3000 cells/well) after treated for 72 h with the indicated doses of PI3K inhibitor (LY294002) and AKT inhibitor (AZD5363). Data are presented as mean  $\pm$  SD ( $n = 3$ ). **C**, Viability assay of H460 and H358 cells expressing control shRNA or NOP56-targeted shRNA (3000 cells/well) after treated for 72 h with the indicated doses of BiP inhibitor (HA15) and ER stress inducer (bortezomib). Data are presented as mean  $\pm$  SD ( $n = 3$ ). **D**, Immunoblots of KRAS-mutant (H358, H460) and wild-type (H1703, H520) cells expressing NOP56-specific sgRNAs. **E**, Viability assay of the cells expressing control or NOP56-specific sgRNAs after treated with rapamycin for 72 h. Data are shown as mean  $\pm$  SD ( $n = 3$ ). **F**, NOP56 is negatively correlated with PI3K/AKT/mTOR pathway genes (*PI3KCA*, *PDPK1*, *PIK3R1*) in KRAS-mutant lung cancer patients. Pearson and Spearman coefficient and significance ( $p$ -value) are analyzed using R software (Cor.test function). **G**, Immunoblots of H460 and H1703 cells expressing control or NOP56-targeted shRNAs. **H, I**, Viability assay of KRAS-mutant (**H**) and wildtype (**I**) cancer cells expressing control or NOP56-specific siRNAs after treated with rapamycin. The assay was performed 72 h after drug treatment (96 h after siRNA transfection). **Figure S4.** NOP56 KD activates and induces dependence on the mTOR pathway in KRAS-mutant cancer cells. **A**, Immunoblots of H358 cells expressing control or NOP56-targeted shRNAs after treated with the AKT inhibitor (AZD5363) for 24 h. **B**, Clonogenic assay of H358 cells expressing control or NOP56-specific shRNAs after treated with indicated doses of AZD5363. Representative images are shown. **C, D**, Immunoblots (**C**) and viability assay (**D**) of H358 cells expressing control or NOP56-specific shRNAs after transfected with *raptor*- or *riCTOR*-specific or control siRNAs for 72 h. Data are presented as mean  $\pm$  SD ( $n = 3$ ). **E**, Clonogenic assay of H358 and H460 cells expressing control shRNA or NOP56-specific shRNAs after



treatment with indicated doses of eIF4E inhibitor (Briciclib). Representative images are shown. **F**, Immunoblots of H460 cells expressing control or NOP56-target shRNAs after treated with rapamycin (1  $\mu$ M) for 24 h. **Figure S5**. In vivo activity and selectivity of co-targeting NOP56 and mTOR in KRAS-mutant lung cancer. **A**, H&E and IHC analysis of p-AKT(T308), p-mTOR(S2448), p-S6(S235/236), Ki67 and Caspase-3) in residual H460 xenograft tumors after the indicated treatment. Scale bars 100  $\mu$ m. **B**, Tumor volume of H1703 xenografts in immunocompromised (NSG) mice. H1703 cells were transduced with either a control or an shRNA against NOP56 (shNOP56a). Tumors were measured every 5 days with a caliper. **C**, Kaplan-Meier survival curve of mice harboring H1703 xenografts from the experiment shown in B.

**Additional file 2: Table S1**. Cell lines used in this study. **Table S2**. Inhibitors used for synthetic lethal chemical screens. **Table S3**. Antibodies used in this study. **Table S4**. KRAS synthetic lethal (SL) genes.

### Acknowledgements

We gratefully acknowledge Christelle Dubey (Division of Thoracic Surgery, Inselspital, Bern University Hospital) for technical support, especially with animal studies and CRISPR-based knockout of NOP56. We thank the West-German Biobank Essen (WBE) for the collaboration in establishment of the PF139 and PF526 lung cancer cells. The Translational Research Unit at the Institute of Pathology, University of Bern is acknowledged for assistance of IHC staining.

### Authors' contributions

ZY, SQL designed and performed the experiments, analyzed the data and wrote the manuscript. LZ, HY performed the experiments and analyzed the data. TMM, BH, YG, BZ, CC and WW analyzed the data and edited the manuscript. PD and GJK provided conceptual inputs, analyzed the data and edited the manuscript. RAS provided financial support and edit the manuscript. RWP conceived the project, supervised the study and wrote the paper. All authors read and approved the final version of the manuscript.

### Funding

This study was supported by a grant from Swiss National Science Foundation (SNSF #310030\_192648; to R-W. Peng) and PhD fellowships from China Scholarship Council (ZY, LZ, YG).

### Availability of data and materials

All data generated or analysed during this study are included in this published article and its supplementary information files.

### Declarations

#### Ethics approval and consent to participate

The establishment of PF139 and PF526 cells was approved by the Ethics Committee of the University Hospital Essen (#18–8208-BO), Germany, with written consents obtained from the patients. The study was performed in accordance with the Declaration of Helsinki. Mouse studies were approved by the Veterinary Office of Canton Bern, Switzerland, and conducted in accordance with Institutional Animal Care.

#### Consent for publication

Not applicable.

#### Competing interests

The authors declare no competing interests.

#### Author details

<sup>1</sup>Division of General Thoracic Surgery and Department of BioMedical Research (DBMR), Inselspital, Bern University Hospital, University of Bern, Murtenstrasse 28, 3008 Bern, Switzerland. <sup>2</sup>Current address: University of Massachusetts Medical School, Worcester, MA 01605, USA. <sup>3</sup>Current address: Department of Thoracic Surgery, Shanghai Chest Hospital, Shanghai Jiao Tong University, Shanghai 200030, China. <sup>4</sup>Department of Thoracic Surgery, University Medicine Essen – Ruhrlandklinik, University Duisburg-Essen, Essen, Germany. <sup>5</sup>Department of Thoracic surgery, Fujian Medical University Union Hospital, Fuzhou City, Fujian, China. <sup>6</sup>Thoracic Surgery Department 2, Hunan Cancer

Hospital and The Affiliated Cancer Hospital of Xiangya School of Medicine, Central South University, Changsha, Hunan, China.

Received: 23 May 2021 Accepted: 1 January 2022

Published online: 17 January 2022

### References

- Prior IA, Lewis PD, Mattos C. A comprehensive survey of Ras mutations in cancer. *Cancer Res*. 2012;72(10):2457–67.
- Reck M, Rabe KF. Precision diagnosis and treatment for advanced non-small-cell lung Cancer. *N Engl J Med*. 2017;377(9):849–61.
- Yang H, Liang SQ, Schmid RA, Peng RW. New horizons in KRAS-mutant lung cancer: dawn after darkness. *Front Oncol*. 2019;9:953.
- Jeanson A, Tomasini P, Souquet-Bressand M, Brandone N, Boucekine M, Grangeon M, et al. Efficacy of immune checkpoint inhibitors in KRAS-mutant non-small cell lung Cancer (NSCLC). *J Thorac Oncol*. 2019;14(6):1095–101.
- Janes MR, Zhang J, Li LS, Hansen R, Peters U, Guo X, et al. Targeting KRAS mutant cancers with a covalent G12C-specific inhibitor. *Cell*. 2018;172(3):578–89.
- Molina-Arcas M, Moore C, Rana S, van Maldegem F, Mugarza E, Romero-Clavijo P, et al. Development of combination therapies to maximize the impact of KRAS-G12C inhibitors in lung cancer. *Sci Transl Med*. 2019;11(510):eaaw7999.
- Ostrem JM, Peters U, Sos ML, Wells JA, Shokat KM. K-Ras(G12C) inhibitors allosterically control GTP affinity and effector interactions. *Nature*. 2013;503(7477):548–51.
- Manchado E, Weissmueller S, Morris JP 4th, Chen CC, Wullenkord R, Lujambio A, et al. A combinatorial strategy for treating KRAS-mutant lung cancer. *Nature*. 2016;534(7609):647–51.
- Shimizu T, Tolcher AW, Papadopoulos KP, Beeram M, Rasco DW, Smith LS, et al. The clinical effect of the dual-targeting strategy involving PI3K/AKT/mTOR and RAS/MEK/ERK pathways in patients with advanced cancer. *Clin Cancer Res*. 2012;18(8):2316–25.
- Huang A, Garraway LA, Ashworth A, Weber B. Synthetic lethality as an engine for cancer drug target discovery. *Nat Rev Drug Discov*. 2020;19(1):23–38.
- Downward J. RAS synthetic lethal screens revisited: still seeking the elusive prize? *Clin Cancer Res*. 2015;21(8):1802–9.
- Luo J, Emanuele MJ, Li D, Creighton CJ, Schlabach MR, Westbrook TF, et al. A genome-wide RNAi screen identifies multiple synthetic lethal interactions with the Ras oncogene. *Cell*. 2009;137(5):835–48.
- De Raedt T, Walton Z, Yecies JL, Li D, Chen Y, Malone CF, et al. Exploiting cancer cell vulnerabilities to develop a combination therapy for ras-driven tumors. *Cancer Cell*. 2011;20(3):400–13.
- Yang Z, Liang SQ, Saliakoura M, Yang H, Vassella E, Konstantinidou G, et al. Synergistic effects of FGFR1 and PLK1 inhibitors target a metabolic liability in KRAS-mutant cancer. *EMBO Mol Med*. 2021;13(9):e13193.
- Martin TD, Cook DR, Choi MY, Li MZ, Haigis KM, Elledge SJ. A role for mitochondrial translation in promotion of viability in K-Ras mutant cells. *Cell Rep*. 2017;20(2):427–38.
- Kim J, McMillan E, Kim HS, Venkateswaran N, Makkar G, Rodriguez-Canales J, et al. XPO1-dependent nuclear export is a druggable vulnerability in KRAS-mutant lung cancer. *Nature*. 2016;538(7623):114–7.
- Nagel R, Semenova EA, Berns A. Drugging the addict: non-oncogene addiction as a target for cancer therapy. *EMBO Rep*. 2016;17(11):1516–31.
- Solimini NL, Luo J, Elledge SJ. Non-oncogene addiction and the stress phenotype of cancer cells. *Cell*. 2007;130(6):986–8.
- Gautier T, Berges T, Tollervey D, Hurt E. Nucleolar KKE/D repeat proteins Nop56p and Nop58p interact with Nop1p and are required for ribosome biogenesis. *Mol Cell Biol*. 1997;17(12):7088–98.
- Newman DR, Kuhn JF, Shanab GM, Maxwell ES. Box C/D snoRNA-associated proteins: two pairs of evolutionarily ancient proteins and possible links to replication and transcription. *RNA*. 2000;6:861–79.
- Cowling VH, Turner SA, Cole MD. Burkitt's lymphoma-associated c-Myc mutations converge on a dramatically altered target gene response and implicate Npl5a/Nop56 in oncogenesis. *Oncogene*. 2014;33(27):3519–27.

22. Su H, Xu T, Ganapathy S, Shadfan M, Long M, Huang TH, et al. Elevated snoRNA biogenesis is essential in breast cancer. *Oncogene*. 2014;33:1348–58.
23. Gong J, et al. A Pan-cancer analysis of the expression and clinical relevance of small nucleolar RNAs in human Cancer. *Cell Rep*. 2017;21(7):1968–81.
24. Pelletier J, Thomas G, Volarevic S. Ribosome biogenesis in cancer: new players and therapeutic avenues. *Nat Rev Cancer*. 2018;18(1):51–63.
25. Bohnsack KE, Bohnsack MT. Uncovering the assembly pathway of human ribosomes and its emerging links to disease. *EMBO J*. 2019;38:e100278.
26. Wang T, Yu H, Hughes NW, Liu B, Kendirli A, Klein K, et al. Gene essentiality profiling reveals gene networks and synthetic lethal interactions with oncogenic Ras. *Cell*. 2017;168:890–903.
27. Weinberg F, Hamanaka R, Wheaton WW, Weinberg S, Joseph J, Lopez M, et al. Mitochondrial metabolism and ROS generation are essential for Kras-mediated tumorigenicity. *Proc Natl Acad Sci U S A*. 2010;107(19):8788–93.
28. Guo JY, Chen HY, Mathew R, Fan J, Strohecker AM, Karsli-Uzunbas G, et al. Activated Ras requires autophagy to maintain oxidative metabolism and tumorigenesis. *Genes Dev*. 2011;25(5):460–70.
29. Yun J, Mullarky E, Lu C, Bosch KN, Kavalier A, Rivera K, et al. Vitamin C selectively kills KRAS and BRAF mutant colorectal cancer cells by targeting GAPDH. *Science*. 2015;350(6266):1391–6.
30. Storz P. KRas, ROS and the initiation of pancreatic cancer. *Small GTPases*. 2017;8(1):38–42.
31. Yang Z, Liang SQ, Yang H, Xu D, Bruggmann R, Gao Y, et al. CRISPR-mediated kinome editing prioritizes a synergistic combination therapy for FGFR1-amplified lung cancer. *Cancer Res Cancer Res*. 2021;81(11):3121–33.
32. Liang SQ, Buhner ED, Berezowska S, Marti TM, Xu D, Froment L, et al. mTOR mediates a mechanism of resistance to chemotherapy and defines a rational combination strategy to treat KRAS-mutant lung cancer. *Oncogene*. 2019;38(5):622–36.
33. Yang H, Liang SQ, Xu D, Yang Z, Marti TM, Gao Y, et al. HSP90/AXL/eIF4E-regulated unfolded protein response as an acquired vulnerability in drug-resistant KRAS-mutant lung cancer. *Oncogenesis*. 2019;8(9):45.
34. El Hassouni B, Sarkisjan D, Vos JC, Giovannetti E, Peters GJ. Targeting the ribosome biogenesis key molecule Fibrillarin to avoid Chemoresistance. *Curr Med Chem*. 2019;26(33):6020–32.
35. Marcel V, Ghayad SE, Belin S, Therizols G, Morel AP, Solano-Gonzalez E, et al. p53 acts as a safeguard of translational control by regulating fibrillarin and rRNA methylation in cancer. *Cancer Cell*. 2013;24(3):318–30.
36. Grade M, Hummon AB, Camps J, Emons G, Spitzner M, Gaedcke J, et al. A genomic strategy for the functional validation of colorectal cancer genes identifies potential therapeutic targets. *Int J Cancer*. 2011;128(5):1069–79.
37. Darling NJ, Cook SJ. The role of MAPK signalling pathways in the response to endoplasmic reticulum stress. *Biochim Biophys Acta*. 1843;2004:2150–63.
38. Hetz C, Zhang K, Kaufman RJ. Mechanisms, regulation and functions of the unfolded protein response. *Nat Rev Mol Cell Biol*. 2020;21(8):421–38.
39. Xu D, Liang SQ, Yang H, Lüthi U, Riether C, Berezowska S, et al. Increased sensitivity to apoptosis upon endoplasmic reticulum stress-induced activation of the unfolded protein response in chemotherapy-resistant malignant pleural mesothelioma. *Br J Cancer*. 2018;119(1):65–75.
40. Cantor JR, Sabatini DM. Cancer cell metabolism: one hallmark, many faces. *Cancer Discov*. 2012;2(10):881–98.
41. DeNicola GM, Karreth FA, Humpton TJ, Gopinathan A, Wei C, Frese K, et al. Oncogene-induced Nrf2 transcription promotes ROS detoxification and tumorigenesis. *Nature*. 2011;475(7354):106–9.
42. Bursać S, Prodan Y, Pullen N, Bartek J, Volarević S. Dysregulated ribosome biogenesis reveals therapeutic liabilities in Cancer. *Trends Cancer*. 2021;7(1):57–76.
43. Bustelo XR, Dosi M. Ribosome biogenesis and cancer: basic and translational challenges. *Curr Opin Genet Dev*. 2018;48:22–9.
44. Justilien V, Ali SA, Jamieson L, Yin N, Cox AD, Der CJ, et al. Ect2-dependent rRNA synthesis is required for KRAS-TRP53-driven lung adenocarcinoma. *Cancer Cell*. 2017;31(2):256–69.
45. Zhou F, Liu Y, Rohde C, Pauli C, Gerloff D, Köhn M, et al. AML1-ETO requires enhanced C/D box snoRNA/RNP formation to induce self-renewal and leukaemia. *Nat Cell Biol*. 2017;19(7):844–55.
46. Albert B, Kos-Braun IC, Henras AK, Dez C, Rueda MP, Zhang X, et al. A ribosome assembly stress response regulates transcription to maintain proteome homeostasis. *Elife*. 2019;8:e45002.
47. Mossmann D, Park S, Hall MN. mTOR signalling and cellular metabolism are mutual determinants in cancer. *Nat Rev Cancer*. 2018;18(12):744–57.
48. Tye BW, Commins N, Ryazanova LV, Wühr M, Springer M, Pincus D, et al. Proteotoxicity from aberrant ribosome biogenesis compromises cell fitness. *Elife*. 2019;8:e43002.
49. Metcalf MG, Higuchi-Sanabria R, Garcia G, Tsui CK, Dillin A. Beyond the cell factory: Homeostatic regulation of and by the UPR<sup>ER</sup>. *Sci Adv*. 2020;6(29):eabb9614.

## Publisher's Note

Springer Nature remains neutral with regard to jurisdictional claims in published maps and institutional affiliations.

**Ready to submit your research? Choose BMC and benefit from:**

- fast, convenient online submission
- thorough peer review by experienced researchers in your field
- rapid publication on acceptance
- support for research data, including large and complex data types
- gold Open Access which fosters wider collaboration and increased citations
- maximum visibility for your research: over 100M website views per year

**At BMC, research is always in progress.**

Learn more [biomedcentral.com/submissions](https://biomedcentral.com/submissions)

